MAX-PLANCK-GESELLSCHAFT

Angewandte Chemie International Edition 51 (2012) 3002-3006

AC FHI

Hydrogen Production by Methanol Steam Reforming on Copper Boosted by Zinc-Assisted Water Activation

C. Rameshan[1,3], W. Stadlmayr[1], S. Penner[1], H. Lorenz[1], N. Memmel[1], M. Hävecker[3], R. Blume[3], D. Teschner[3], T. Rocha[3], D. Zemlyanov[2], A. Knop-Gericke[2], R. Schlögl[3], B. Klötzer[1]*

[1]Institute of Physical Chemistry, University of Innsbruck, Innrain 52A, 6020 Innsbruck (Austria)
[2]Birck Nanotechnology Center, Purdue University, 1205 West State Street, West Lafayette, IN 47907-2057 (USA)
[3]Department of Inorganic Chemistry, Fritz Haber Institute of the Max Planck Society, Faradayweg 4-6, 14195 Berlin (Germany)

* Corresponding author: e-mail bernhard.kloetzer@uibk.ac.at,

Received 16 September 2011; Revised 14 November 2011; Issue published online 13 March 2012

Keywords: copper/zinc alloys;methanol steam reforming;surface chemistry;water activation;X-ray photoelectron spectroscopy

For use of polymer electrolyte membrane fuel cells (PEMFC) in mobile power applications, an efficient source of CO-depleted hydrogen is needed. To avoid technical and safety problems of hydrogen handling, storage and transport, methanol can be used as practical and abundant energy carrier for on-board H_2 generation, having the advantage of high energy density. Hydrogen generation from methanol can be performed by catalytic methanol steam reforming (MSR): $CH_3OH + H_2O \rightarrow CO_2 + 3H_2$. Methanol conversion must be carried out with very high CO_2/H_2 selectivity, in order to avoid CO-poisoning of the fuel cell anode. A number of promising selective MSR catalysts are available. Apart from advanced copper-based catalysts,[1-2] special attention is presently paid to the highly MSR-selective reduced state of Pd/ZnO,[3] containing a particularly stable intermetallic PdZn (1:1) active phase.[3-4] Therefore, we recently studied related "inverse" near-surface PdZn intermetallic phases, showing that three-dimensional PdZn active site ensembles are equally important for selective dehydrogenation of methanol (thus avoiding CO) and for efficient water activation.[5] For the less costly Cu/ZnO catalysts, originally designed for methanol synthesis, still improvements towards a technical MSR application regarding sintering stability, pyrophoricity and selectivity are required. Empirical development of Cu/ZnO catalyst preparation and -activation has aimed in a particularly large Cu^0-ZnO contact.[6] Nevertheless, on technical catalysts it is very difficult to derive an unambiguous causality for the contact's role. A beneficial function of Zn is quite obvious to the community, but a clear assignment of a predominant promotional effect (both from the theoretical and experimental side) is still missing. From the Cu/ZnO literature one can choose between seemingly incompatible model interpretations, involving the „metallic copper model",[7] the „special site model",[8] the „morphology model",[7,9] the „spillover model",[10] and last but not least the „Cu–Zn alloy model".[8,11] Consequently, the Cu-ZnO(H) contact most likely constitutes a combination of promotional effects. The central aim of our study is to highlight the aspect of Zn-promoted water activation. This is achieved by using an ultrahigh vacuum (UHV) "inverse" model catalyst approach, which – in contrast to investigations on real catalyst systems – allows to better follow the Zn-segregation behaviour and the changes in redox chemistry of both Cu and Zn. This provides a solid basis for directional promotion of microkinetic steps leading to enhanced CO_2-selectivity.

In practice, a series of CuZn near-surface alloy and bulk brass samples were tested. The near-surface alloy preparations on Cu foil involved variable thermal Zn evaporation and thermal annealing conditions. Commercial bulk brass foil samples with 10 to 37 weight % Zn content were cleaned by usual UHV procedures. The respective bimetallic pre-reaction state was characterised by depth-resolved XPS and AES analysis of the alloy composition. Then, quantitative kinetic MSR reaction studies were perfomed in

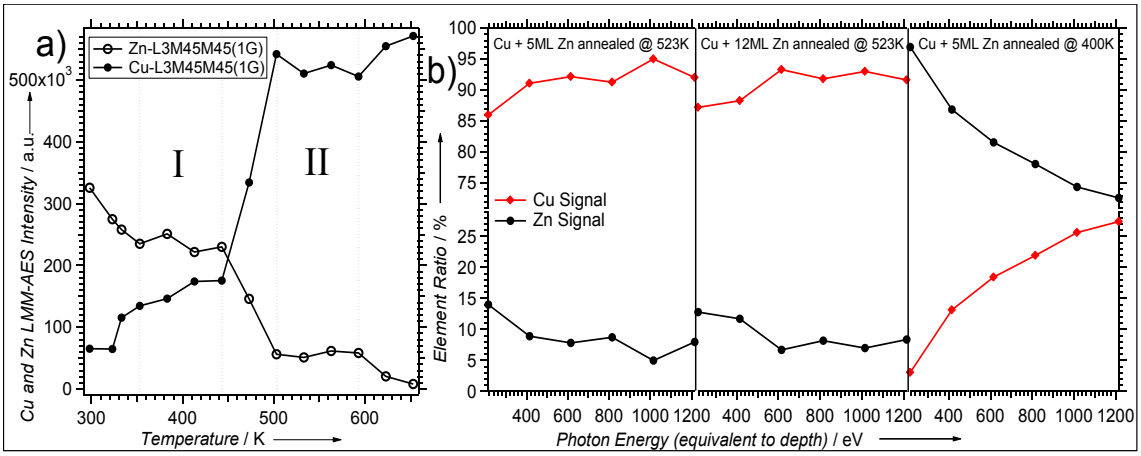

Figure 1: (a) Peak-to-peak intensities (a.u.) of the differentiated Zn-$L_3M_{45}M_{45}$ and Cu-$L_3M_{45}M_{45}$ Auger peaks as function of annealing temperature. Initially 12 ML of Zink were deposited at ~300K on clean Cu foil and annealed for 5 min at the respective temperature. (b) Element ratio of Cu and Zn (in %) in dependence of the analysis depth, derived from the Cu3p and Zn3p XPS signals (depth profile by photon energy variation from 215 to 1215 eV, corresponding to ~0.5 – 1.3 nm IMFP of photoelectrons). Preparation conditions: evaporation of 5 or 12 ML of Zink at ~300K followed by thermal annealing at 400K or 523K.

an UHV-compatible all-glass reaction cell operating between 10^{-10} and 1000 mbar. Finally, simultaneous "in-situ" analysis using product detection by mass spectrometry and ambient pressure X-ray photoemission spectroscopy (AP-XPS) was performed at the HZB/BESSY II synchrotron (details given in the experimental section, supporting information). On this basis we are able to show that the CO_2-selectivity and activity in MSR strongly scales with the available $Cu(Zn)^0$/Zn(ox) interface, which forms in-situ by partial oxidative Zn segregation in the MSR gas phase on a suitable near-surface alloy "pre-catalyst". In this context we emphasize that the *exact degree of initial Zn-doping* is crucial to establish a maximum $Cu(Zn)^0$/Zn(ox) interface and thus activity. Water activation and total oxidation toward CO_2 is inhibited on bulk- and surface-clean, thermally annealed, structurally equilibrated copper foil, representing a particularly unreactive state of Cu (for a brief discussion of potential Cu activators other than Zn see supporting information S5). But also initially too Zn-rich near-surface alloys and all investigated bulk brass samples showed complete deactivation by Zn(ox) surface passivation. By systematic variation of the Zn amount and of the annealing temperature, the most active and selective CuZn near-surface alloy preparation was empirically identified: evaporation of 5 to 12 monolayers (ML) of Zn onto Cu foil at 300K, followed by thermal annealing in vacuum at 523 K for 10 min.

In order to characterise the optimized bimetallic "pre-catalyst", 5 or 12 ML Zn were deposited under UHV conditions onto clean Cu foil at ~300K, followed by stepwise thermal annealing up to 653K. The corresponding Auger electron spectroscopic (AES) effects are shown in Figure 1a. Two stability plateaus are discernible. It is evident that annealing at ~400 K gives rise to a ~4 times higher Zn concentration within the first few layers of the sample than annealing at 500 K and above. The approximate Cu:Zn=9:1 intensity ratio after annealing at 500 K and beyond can be used to estimate the mean Zn content of the AES-visible near-surface regions (kinetic energies of LMM-Auger transitions: 920 eV (Cu) and 994 eV (Zn), IMFP ~1.4 nm for Cu, ~1.6 nm for Zn at 900-1000 eV[12]). Assuming an extremely "flat" Zn-in-Cu concentration gradient for 523K annealing, which is verified by the XPS depth profiling data of Figure 1b, quantification of the AES results can be attempted without considering variable intensity contribution with increasing probe depth. Moreover, the AES transitions were excitated using MgK_a radiation, thus as a reasonable approximation for the relative Auger sensitivities the respective Cu2p and Zn2p XPS cross sections can be used. On this basis a Cu:Zn ratio of ~10:1 was estimated for the relatively narrow surface region detected by AES. As 12 ML of Zn at this ratio corresponds to a thickness of a 10:1 alloy region on top of the deeper Cu bulk of ~31nm (~12*10*0.26nm), any concentration gradient within the first few layers and any gradient-dependent intensity attenuation can be neglected. The same estimation, applied to the 400K - 450K annealed state, results in a ~45:55 Cu:Zn ratio, suggesting the presence of a b-brass layer (region I in Figure 1a) becoming thermally unstable above 450 K. In the range 450K – 500K the transition from near-surface b-brass to a-brass (region II in Figure 1a) occurs, and finally a thermal stability range of the near-surface a-brass state between 500 K and 600 K can be deduced from Figure 1. Naturally, due to the presence of the almost infinite Cu bulk as nearby diffusional "sink", the stability ranges of the near-surface alloys are strongly shifted to low temperatures, in comparison to their bulk counterparts.

To back-up the AES quantification of the Zn content and -gradient within the near-surface region, variation of the

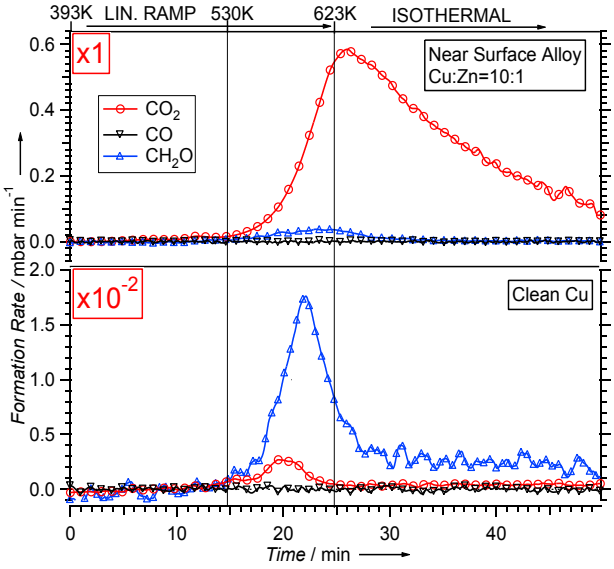

Figure 2: Temperature-programmed MSR on the CuZn~10:1 near-surface alloy (upper panel) versus clean Cu foil (lower panel). Reaction conditions: 12 mbar methanol, 24 mbar water, 977 mbar He; linear temperature ramp (9.0 K/min) up to 623K, followed by isothermal reaction for 25 min. The decrease of the CO_2 formation rate in the isothermal region is caused by progressive reactant consumption (methanol conversion after 50 min: ~85%).

XPS probe depth by photon energy variation was performed. Figure 1b shows the large differences in the resulting Zn near-surface distribution between annealing of 5ML Zn below ~450 K and above 503 K, followed by contact to the ambient at ~298 K. For annealing at 523 K, the Cu:Zn~10:1 estimation derived from Figure 1a is complemented by a Cu:Zn~12:1 estimation for deeper layers of the 5 and 12 ML preparations, and only the outermost region showed minor oxidative Zn-enrichment.

The MSR activity/selectivity of the CuZn~10:1 alloy was quantitatively studied in comparison to clean Cu by temperature-programmed reaction in an UHV-compatible high pressure cell operated as recirculating batch reactor under realistic reaction conditions. Figure 2 (upper panel) reveals that the CuZn~10:1 surface alloy quickly converts CH_3OH and water to CO_2 and formaldehyde (CH_2O) with virually no CO formation in the entire temperature region between 530K and 623K, which is the upper limit in the batch reactor tests. In contrast, on clean Cu hardly any conversion of methanol is observed.

An activation energy of ~93 kJ/mole for CO_2 formation was estimated from the initial rate increase (see supporting information, Fig. S1). At ~600K, CH_2O is formed on both catalysts to some extent, but only on CuZn~10:1 a high activity/selectivity toward CO_2 is present. Clean Cu only catalyzes the selective dehydrogenation of methanol to formaldehyde. Hence the balance of dehydrogenation vs. subsequent total oxidation by water governs the CH_2O:CO_2 product ratio. A strong kinetic inhibition of water activation on clean, unactivated Cu can thus explain the huge difference to the CO_2-active CuZn system.

The MSR-induced segregation behaviour of initial CuZn~10:1 at ambient reactant pressure between 300K and 543K is illustrated in Figure 3 by the Zn3d and Cu3d valence band XPS spectra acquired *in situ*. Starting at 300 K from the bimetallic state (Figure 3a), already heating to 453 K induces a Zn3d shift toward higher binding energy (BE) and a pronounced relative increase of Zn3d vs. Cu3d intensity, indicating the onset of oxidative Zn segregation to the surface. Up to 543K, the gradual transition from the bimetallic state to a mixed Zn(bimetal)-Zn(ox) state further proceeds, as can be deduced from the respective Zn3d peak deconvolution in Figure 3b showing approximately equal contributions of bimetallic and oxidised Zn around 550 K (for details of the deconvolution procedure see supporting information S2). The fact that the Zn3d/Cu3d atom ratio also increases from ~0.13 at 300 K up to a value of ~0.36 at 543 K (detailed temperature dependence of Zn/Cu ratio shown in Fig. S2(a), supporting information), is interpreted in terms of optimized surface wetting of $Cu(Zn)^0$ by "interfacial Zn(ox)", rather than purely 3-dimensional growth of bulk ZnO islands, which would be much less sensitively detected at hn=130eV. The roughly equal contributions of oxidised and bimetallic Zn3d components, in combination with the pronounced Zn:Cu intensity maximum at 543 K, suggest that the evolving active state is characterized by the presence of an only partially $Cu(Zn)^0$-blocking Zn(ox) layer with a maximum number of $Cu(Zn)^0$-Zn(ox) interfacial active sites. At 543 K, also the onset of CO_2 formation on initial CuZn~10:1 is evident from Figure 2 (upper panel).

Nevertheless, the exact spatial distribution of "interfacial Zn(ox)" (local ensembles consisting of a few atoms vs. extended, more or less flat islands) and the predominant Zn-coordination chemistry within (distribution of Zn-Cu^0, Zn-O and Zn-OH bonds) remains to be clarified.

At temperatures above 543K, progressive Zn (intensity) loss is obvious from Figures 3c and 3d, whereas the Zn3d BE maximum position still shifts further up till ~11. 5 eV. Complete loss of the bimetallic Zn component is evident at >633K in Figure 3d, whereas total loss of all Zn is evident from the 723K spectrum in Figure 3c. As the pathways to reduce surface Zn intensity are 3-dimensional clustering of Zn(ox) and/or reduction of Zn(ox) to Zn^0, either followed by diffusion into the deep bulk or by desorption, we presently can only suggest a combination of these processes. However, Zn intensity loss relative to Cu^0 necessarily means loss of active Cu^0/Zn(ox) interface, both if 3-dimensional clustering or reductive Zn loss dominates.

We strongly emphasize the absence of detectable amounts of oxidised Cu species under reaction conditions, as evident from all Cu-XPS-regions (see e.g. the largely invariant "metallic" Cu3d region in Figures 3a and 3c).
This is also supported by the O1s intensity trend, which closely tracks the behaviour of the Zn(ox) intensity (for details see supporting information S4). Moreover, a continous O1s-trend to higher BE from 531.2 eV to ~533 eV

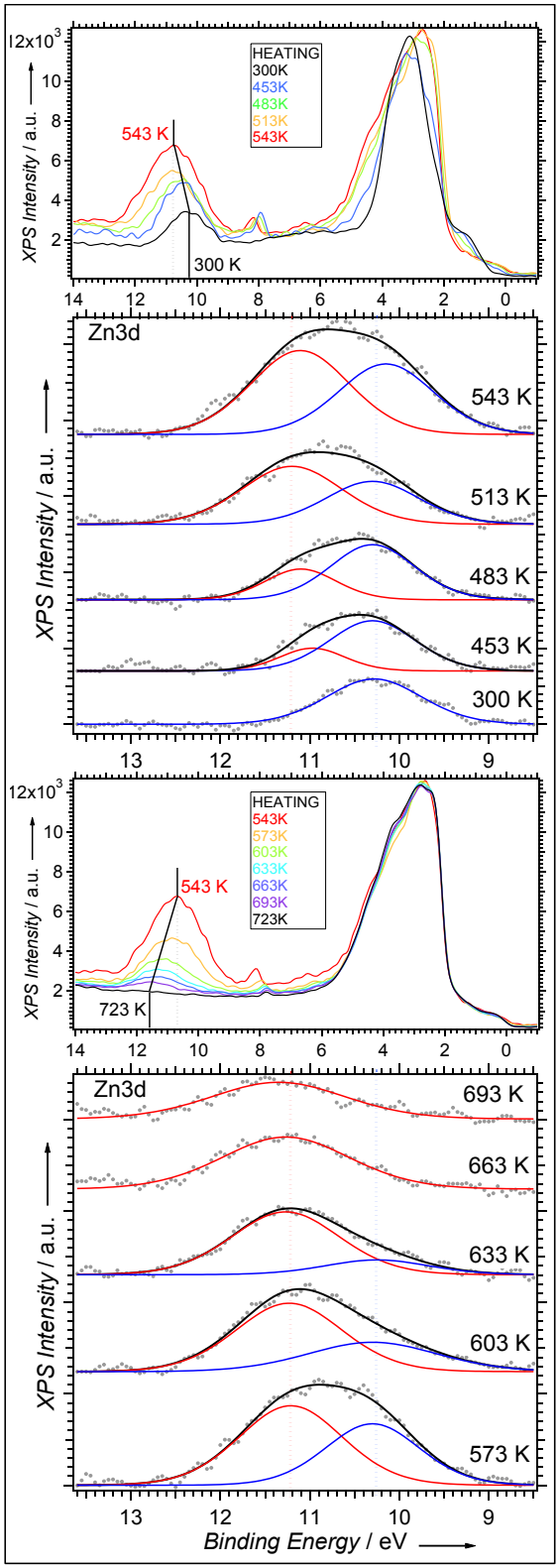

Figure 3: (a) and (c): AP-XPS spectra (Zn3d and Cu3d regions) recorded at hn=130eV *in situ* during MSR (0,12 mbar methanol + 0,24 mbar water) starting from CuZn~10:1. Corresponding Zn3d peak deconvolution in (b) and (d): red, BE~11.2 eV: Zn(ox); blue, BE~10.25 eV: bimetallic ZnCu (details of Zn3d binding energy and intensity trends given in supporting information S2).

between 453 K and 723 K is interpreted in terms of an increasing contribution of hydroxylated surface species (ZnO ~531.6 eV vs. Zn(OH) ~533.5 eV,[13] Cu-OH ~531.9 eV and adsorbed water ~533.0 eV[14]). A gradual change of the $Cu(Zn)^0$/Zn(ox) active state to a less active Zn-depleted, but partially hydroxylated, Cu^0 state above 633 K is also inferred from the less-than-exponential temperature dependence of the reforming activity above 633 K. Since at ~700K total Zn loss is evident (Figure 3c), the residual reforming rate, combined with a BE as high as 533 eV for O1s, is attributed to the now activated Cu foil covered by a rather small amount of reactive OH groups (details given in supporting information S5).

In conclusion, the Cu:Zn~10:1 „pre-catalyst“ state provides an appropriate near-surface Zn loading for MSR-induced segregation to yield submonolayer Zn(ox) coverages and therefore a high abundance of bimetal-$Cu(Zn)^0$/Zn(ox) interface at ~550 K, as depicted in Scheme 1. This, in turn, creates optimized conditions for bifunctional catalyst operation: $Cu(Zn)^0$ regions favour selective methanol dehydrogenation to formaldehyde, whereas redox-active $Cu(Zn)^0$-Zn(ox) sites[8,15] assist in water activation and the transfer of hydroxide or oxygen to the latter, thus providing optimum conditions for high CO_2-activity and -selectivity.

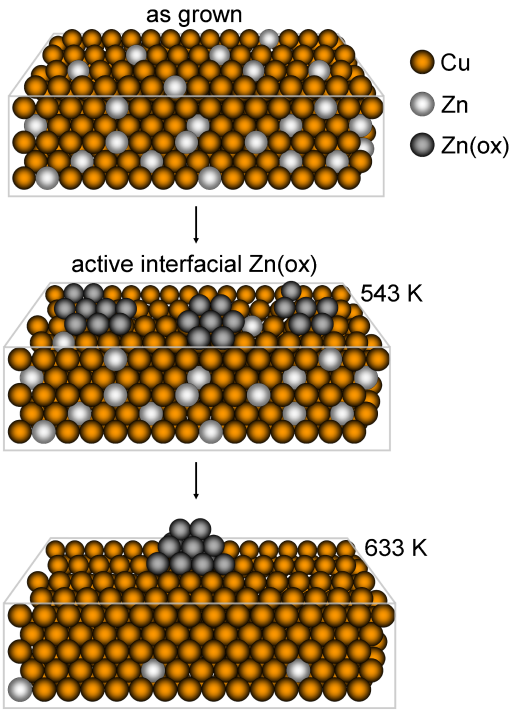

Scheme 1: Upper panel: pre-catalytic “as-grown” 10:1~CuZn bimetallic state. Middle panel: superior “in-situ” active surface state with maximum wetting of $Cu(Zn)^0$ by interfacial Zn(ox). Lower panel: High temperature state after major Zn intensity loss by 3-dimensional Zn(ox) clustering and/or bulk diffusion/ desorption of Zn^0.

On clean and unactivated Cu foil, dehydrogenation ceases with formaldehyde, but also fully Cu^0-blocking Zn(ox) coverages cause complete deactivation.

As a perspective for future research, the detailed reaction mechanism of CO_2 formation from water-derived -O or -OH species and formaldehyde remains to be clarified. So far, intermediates originally predicted for the metallic Cu^0 surface, such as dioxomethylene[16-17] and hydroxymethoxy, which was recently proposed in between formic acid and formaldehyde,[18] remain to be verified or disproved. Consequently it is important to study not only bimetallic $Cu(Zn)^0$ sites, but also interfacial $Cu(Zn)^0$/Zn(ox)- and Zn(ox) surface sites. Finally, the role of reactive formate intermediates, again on (bi)metallic, oxidic and interfacial sites, should be studied in more detail. Promotion of formate reactivity has already been reported both for Zn-modified[8] and O_{ads} modified Cu(111).[19] The high specific methanol synthesis activity of Cu/ZnO catalysts was previously ascribed to a-brass formation.[20] In this context, „bridging" formate species located at special Cu-Zn sites were reported.[21]

As the main advantage of our model system is both a high abundance and a close spatial vicinity of bifunctional active surface regions, we emphasize possible implications for selectivity tuning of Cu-Zn-based „real" MSR catalysts. Based on controlled Zn(ox) segregation from sufficiently diluted bimetallic Zn-in-Cu precursors to yield a similar $Cu(Zn)^0$ – Zn(ox) surface microstructure, the directional promotion of formaldehyde total oxidation, combined with enhanced decarboxylation selectivity of Cu-Zn-bonded formate species to suppress CO, appears feasible.

References

[1] a) J. Argell, H. Birgersson, M. Boutonnet, I. Melián-Cabrera, R.M. Navarro, J.L.G. Fierro, *J. Catal.* **2003**, 219, 389; b) M. Behrens, S. Kissner, F. Girsgdies, I. Kasatkin, F. Hermerschmidt, K. Mette, H. Ruland, M. Muhler, R. Schlögl, *Chem. Commun.* **2011**, 47(6), 1701.
[2] H. Purnama, F. Girgsdies, T. Ressler, J.H. Schattka, R.A. Caruso, R. Schomäcker, R. Schlögl, *Catal. Lett.* **2004**, 94 (1-2), 61.
[3] N. Iwasa, N. Takezawa, *Top. Catal.* **2006**, 22, 215.
[4] S. Penner, B. Jenewein, H. Gabasch, B. Klötzer, D. Wang, A. Knop-Gericke, R. Schlögl, K. Hayek, *J. Catal.* **2006**, 241, 14.
[5] C. Rameshan, W. Stadlmayr, C. Weilach, S. Penner, H. Lorenz, M. Hävecker, R. Blume, T. Rocha, D. Teschner, A. Knop-Gericke, R. Schlögl, N. Memmel, D. Zemlyanov, G. Rupprechter, B. Klötzer, *Angew. Chem. Int. Ed.* **2010**, 49, 3224.
[6] I. Kasatkin, P. Kurr, B. Kniep, A. Trunschke, R. Schlögl, *Angew. Chem.* **2007**, 119, 7465.
[7] J.D. Grunwaldt, A.M. Molenbroek, N.Y. Topsøe, H. Topsøe, B.S. Clausen, *J. Catal.* **2000**, 194, 452.
[8] J. Nakamura, Y. Choi, T. Fujitani, *Top. Catal.* **2003**, 22, 277.
[9] K.C. Waugh, *Catal. Lett.* **1999**, 58, 163.
[10] M.S. Spencer, *Catal. Lett.* **1998**, 50, 37.
[11] M. Sano, T. Adaniya, T. Fujitani, J. Nakamura, *J. Phys. Chem. B* **2002**, 106, 7627.
[12] S. Tanuma, T. Shiratori, T. Kimura, K. Goto, S. Ichimura, C.J. Powell, *Surf. Interface Anal.* **2005**, 37, 833.
[13] M. Kunat, St. Gil Girol, U. Burghaus, Ch. Wöll, *J. Phys. Chem. B* **2003**, 107, 14350.
[14] I. Platzman, R. Brener, H. Haick, R. Tannenbaum, *J. Phys. Chem. C* **2008**, 112, 1101.
[15] T.V. Herwijnen, W.A.D. Jong, *J. Catal.* **1974**, 34, 209.
[16] Z.-M. Hu, H. Nakatsuji, *Chem. Phys. Lett.* **1999**, 313(1,2), 14.
[17] K. Takahashi, N. Takezawa, H. Kobayashi, *Appl. Catal.* **1982**, 2(6), 363.
[18] L.C. Grabow, M. Mavrikakis, *ACS Catalysis* **2011**, 1(4), 365.
[19] Y. Yang, C.A. Mims, R.S. Disselkamp, J.-H. Kwak, C.H.F. Peden, C.T. Campbell, *J. Phys. Chem. C* **2010**, 114, 17205.
[20] a) M.S. Spencer, *Surf. Sci.* **1987**, 192, 323; b) M.S. Spencer, *Surf. Sci.* **1987**, 192, 329; c) M.S. Spencer, *Surf. Sci.* **1987**, 192, 336.
[21] a) J.E. Bailie, C.H. Rochester, G.J. Millar, *Catal. Lett.* **1995**, 31, 333; b) K.M.V. Bussche, G.F. Froment, *Appl. Catal. A* **1994**, 112, 37.

Preprint of the Department of Inorganic Chemistry, Fritz-Haber-Institute of the MPG *(for personal use only)* (www.fhi-berlin.mpg.de/ac)